Effects of Concentration on the Sensing Properties of Rgo/ Cuo Nanoparticles as Ammonia Gas Sensor

Inam A. Hammod[1,2], Noor J. Ridha[1], Khawla J. Tahir[1], Firas K. Mohamad Alosfur[1], Asaad S. Yasir[1]

[1] Department of Physics, College of Science, University of Kerbala, Karbala, Iraq.
[2] Department of Physiology and Medical Physics, College of Medicine, University of Kerbala, Karbala, Iraq.
E-mail: inam.a@uokerbala.edu.

This study proposed a low-cost and straightforward hydrothermal method to prepare reduced graphene oxide/copper oxide (rGO/CuO) nanocomposites at 100 ℃ for different amounts of rGO. In this method, the reduction of graphene oxide and the formation of copper oxide occur using NaOH as the reducing agent at low temperatures, and then the structural, morphological, and optical properties are evaluated. The results of XRD showed that the prominent peaks related to the formation of rGO/CuO were observed. The particle size of nanoparticles was calculated and found to increase after annealing to 400 ℃. The morphological results revealed the formation of two structures, rod and spherical- shape, according to the difference in the GO ratios in the nanocomposites. The results of TGA illustrated the thermal stability of rGO/CuO compared to pure GO. They showed that the stability depends on the GO concentration in the nanocomposite, which decreased with increasing GO concentration. The fabricated sensors with pure CuO and rGO/CuO composites were tested for ammonia detection at different temperatures. The rGO/CuO nanocomposites sensor showed a three-fold improvement in sensor response compared to a bare CuO sensor at room temperature, in addition to rapid response and recovery time of about 21seconds and 15 seconds, respectively.

Keywords: N Reduced graphene oxide, copper oxide, gas sensor, and hydrothermal method, sensitivity.

1. Introduction

Nanoscience and nanotechnology refer to the production, characterization, and development of the applications of tiny particles ranging between 1 and 100 nm. 1,2,3. Among nanoparticles, metal oxide nanoparticles have become very popular in recent decades due to

their amazing properties. 4,5,6. Copper oxide (CuO) has good magnetic, electrical, physical, and optical properties. It has attracted considerable attention in a variety of applications, including improved photocatalytic activity 7,8,9 supercapacitor applications 1011, and gas sensors 12,13. CuO is a p-type semiconductor with a band gap of 1.2 eV, a melting point of 1330 °C and a density of 6.4 g〖cm〗^(-3). CuO can be found in two important phases: cupric oxide (CuO) and cuprous oxide (Cu2O) 14. CuO can be synthesized by various methods such as chemical vapor deposition (CVD), sol-gel, spray pyrolysis, hydrothermal, pulsed laser deposition, etc. Depending on the physical or chemical strategies used, different sizes, dimensions and morphologies can be obtained 15. More stable phase of CuO can exist in numerous forms, such as nanoparticles, nanoplates, nanowires, nanoneedles, nanorods, nanoflowers and thin films 16. On the other hand, CuO lacks excellent electrical conductivity and rapid capacity decay, and its mechanical properties are limited compared to other oxides 17,18. Therefore, researchers have made many efforts to overcome its disadvantages by controlling the geometry of the nanostructure or by functionalization 19. Functionalization is a way to change the chemical characterization of a material by bringing nanoparticles into contact with the surface of a material, thereby introducing additional features and changing the surface chemistry of the material 20,21. Graphene oxide (GO) and reduced graphene oxide (rGO) have been suggested as promising candidates to improve CuO characterizations because of their superior thermal, electrical, and mechanical qualities 22 in addition to their size in the range of nanometer, large surface to volume ratio, and limited toxicity 23. Graphene is a two-dimensional hexagonal structure that can be oxidized to obtain GO, which is considered one of the best oxides used in recent years, with an energy gap of 2.2 eV 24. GO is a single-layer flake with more oxygen functional groups, easily dissolving in water and other solvents 25. This property is helpful in electronic applications 26. GO can be thermally or chemically reduced to obtain rGO. rGO will help improve its applications. The graphene derivatives are versatile materials and, therefore, could be used in various fields such as photovoltaic applications 27, nanomedicine 28, intelligent drugs 29,30, organic solar cells 31, and gas sensing 32. Various methods have been investigated for the synthesis of rGO/CuO and studied their properties and applications. Chandrama Sarkar and Swapan K. Dolui 33 achieved the preparation of CuO/rGO by hydrothermal method at 150 ℃ and explained the role of the catalyst in the reduction of 4/ NP. It was found from the results of FTIR and XRD that a weak diffraction peak related to rGO was observed and crumpled- like paper- surface of GO incorporated with Cu nanoparticles. Jae-Hun Kima et al. 34 synthesized CuO/rGO by electrospinning using copper acetate as a precursor. In this study, different ratios of rGO were loaded with CuO and showed an excellent response for H2S gas. In this area, rGO with p-type CuO can be an amazing materials. Dongzhi Zhang et al. 35 prepared a sensing film of rGO/CuO by hydrothermal method treated at 180 ℃ for 18 hours. In this work, the configuration includes three layers of rGO-CuO-rGO oxides exhibted best response for hydrogen gas than pure rGO or CuO. On the other hand, Suresh Sagadevan et al. 36 fabricated rGO-CuO in facile chemical method using reducing agent like N-dimethyl-formamide and ammonia. The SEM and TEM results showed that the particles in the spherical- shape with averge size in the range of 60 nm. Based on the electrochemical data, the CuO/rGO nanocomposite shows great potential as a highly effective material for supercapacitor electronics. M. Iniya Pratheepa et al. 37 utilized NaOH as a reducing agent for reduction of CuO/rGO by chemical method. The FTIR findings confirmed the formation CuO/rGO with

band gap of 2.1 eV. The excellent electrochemical -capacitive conductivity of the produced rGO/CuO nanoparticles makes them an ideal electrode material for supercapacitors with high-performance. Semiconductor sensors, with low power consumption and excellent resistance measurement, are widely utilized in environmental, agricultural, industrial, energy, and medicine monitoring applications. Nanomaterials like CuO and rGO are widely used in semiconductor gas sensors. This is because rGO exhibits favorable physical and chemical characteristics that were mentioned previously. These attributes are advantageous for gas adsorption and redox reactions on the material's surface, which can be considered a main factor in enhancing the gas sensors' performance. Moreover, the heterojunctions formed by combining metal oxides with rGO can offer a pathways for carrier transport, leading to an increased number of active sites for gas adsorption 38. Industrial exhausts and wastes emit hazardous gases like ammonia (NH3), hydrogen sulfide (H2S), and carbon monoxide (CO), etc, leading to chronic health issues. This might significantly affect employees of life. Monitor these gasses regularly to ensure employee safety 39. NH3 gas is a poisonous, colorless, and odorous gas that widely used in several industries, such as environmental, automotive, industrial, chemistry, and medical diagnostics. Ammonia is corrosive and extremely toxic, causing damage to the lungs, eyes, skin, and pharynx of those who inhale it. As a result, exceeding the acceptable inhalation level is of utmost importance to prevent contracting life-threatening illnesses 40. In this work, the reduction of GO and the production of rGO/CuO can be carried out by hydrothermal process at low temperature (100 °C) for four hours without any reducing agents. The influence of the preparation temperature on the reduction process was also investigated. Different amount of rGO were loaded with CuO to evaluate its effect on the carecterization of the nanocomposites. The nanocomposites were annealed at 400 °C for two hours and the effect of annealing on the structure and morphology was explained in detail. Additionally, we report on the dynamic response of rGO/CuO nanocomposites when exposed to NH3 gas concentrations of 100 ppm at different operation temperatures.

2. Materials

GO, Cu (No3)2.3H2O and NaOH were purchased from BDH Chemicals Ltd Poole England, ALPHA CHEMIKA in INDIA.

Preparation methods

Preparation of reduced graphene oxide:

To thermally reduce GO, 2 gram of GO powder was dissolved in 100 mL of deionized water and sonicated for 30 minutes until all the powder was dispersed. This solution was then stirred for another 30 minutes, transferred to a sealed 100 mL autoclave, and heated in the oven at 100 °C for 4 hours. The product was washed five times with ethanol and distilled water, then dried at 100 °C for 2 hours according to equation 41:

$$\mathrm{GO} \rightarrow \mathrm{rGO} + \mathrm{CO}\uparrow + \mathrm{CO_2}\uparrow + \mathrm{H_2O}\uparrow \quad (1)$$

Finally, the as-prepared nanocomposite was annealed in the electric furnace for 2 hours at 400 °C for further characterization.

Preparation of copper oxide:

To prepare CuO using the same method, 2 gram of Cu(NO3)2.3H2O was dissolved in 100 mL of deionized water and sonicated for 30 minutes. The color of a solution turns blue. Then (1 M) NaOH was slowly added with continuous stirring for another 30 minutes. The pH of the composites was tested and recorded to be 10. The solution was transferred to a 100 mL autoclave and heated at 100 °C for 4 hours. The obtained product was washed five times with ethanol and distilled water and then dried at 100° C for 2 hours. This reaction can be described as follows:

$$Cu(NO_3)_2 + 2\,NaOH \rightarrow Cu(OH)_2 + 2\,NaNO_3 \quad (2)$$

$$Cu(OH)_2 \rightarrow CuO + H_2O \quad (3)$$

The as-prepared nanocomposite was annealed in the electric furnace for 2 hours at 400 °C for further characterization.

Preparation of reduced graphene oxide-copper oxide:

rGO/CuO was prepared using a hydrothermal process. First, a certain amount of GO powder was ultrasonically dispersed in 100 mL of deionized water for 30 minutes until the solution became homogeneous and brown. Then, 2 gram of Cu(NO3)2.3H2O was added to the obtained dispersion and stirred for 15 minutes. After that, (1 M) NaOH was slowly added with continuous stirring for another 20 minutes. The pH of the composites was tested and reported to be 9. Finally, the resulting mixture was transferred to a sealed 100 mL autoclave and heated in the oven at 100 °C for 4 hours. The composite was rinsed with ethanol and deionized water five times until pH 7 was attained. The final product was dried at 100 °C for 2 hours. The schematic diagram of the fabrication process is shown in (Figure 1). Different amounts of GO (0.5 gram, 1 gram, 2 gram) were used to explain its effect on the nanocomposites. The three samples were annealed in the electric furnace for 2 hours at 400 °C for further characterization.

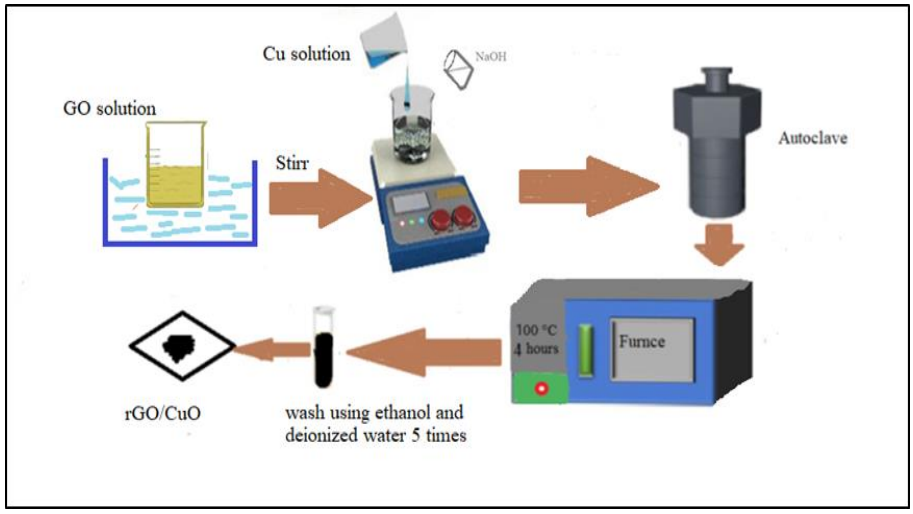

Figure1. Schematic diagram of the preparation process of rGO/CuO.

3. Characterization

The morphological, structural, elemental, and optical properties of the prepared composite were identified using field emission scanning electron microscopy (FESEM), X-ray diffraction (XRD), energy dispersive X-ray spectroscopy, elemental mapping (EDX), UV-visible spectroscopy, Fourier transform infrared spectroscopy (FTIR), and thermogravimetric analysis (TGA). The size of the crystallite D can be calculated using Scherer's equation 42,43:

$$D = \frac{K\,\lambda}{\mathrm{B}\cos\theta} \qquad (1)$$

Where D is the crystallite size in (nm); K is the shape factor (0.94); λ is the wavelength of the X-rays (1.5064 A); B is half the maximum of full width. In addition, thermogravimetric analysis (TGA) tests are used to study the thermal stability of materials.

Fabrication of sensors

The glass was chosen as the substrate for depositing CuO and rGO/ CuO samples. A 2.5 cm × 2.5 cm glass substrate was cleaned with distilled water and alcohol, followed by 30 minutes of sonication, then dried on a hot plate for 10 minutes. The dip coating process was chosen for thin film deposition due to its ease of use and low cost. 100 mL was taken from each sample and placed in a baker. Glass substrates were immersed in a beaker containing solutions with an average velocity of 0.11 mm/s. The process entailed keeping the substrate in the beaker for 5 minutes and then withdrawing the sample at the same speed. Finally, the samples were dried on a hot plate at 90 ℃ for 10 minutes. The method is repeated five times for each sample to achieve a homogeneous thin coating. The deposited films are annealed in an electric furnace at 400℃ for two hours. During the sensor fabrication process, two electrodes were sputtered onto the surface of the thin films using an appropriate mask. Gold fringe-shaped electrodes with a finger spacing of 400 µm and a fringe width of 350 µm were used. The schematic diagram of the semiconductor sensor is shown in Figure 2.

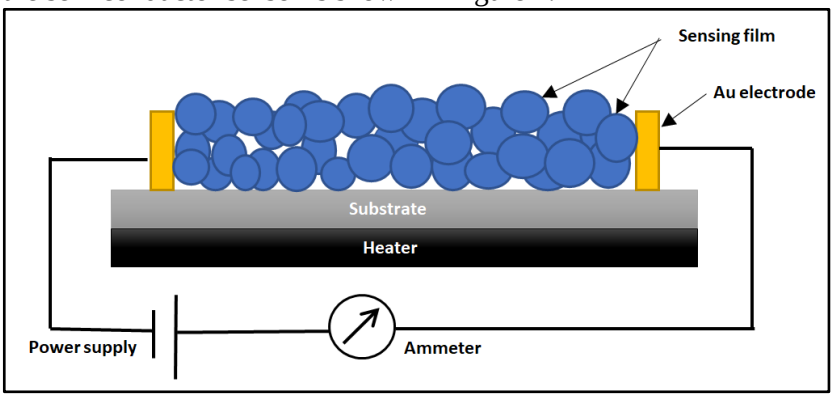

Figure 2. Schematic diagram of semiconductor sensor.

Measurement of Gas-Sensing

A handmade testing system was used to evaluate the detection and characterization of CuO and rGO/ rGO sensors. NH3 gas was diluted with nitrogen and put into the enclosed chamber. Track NH3 concentration with a mass flow meter and control it by air dilution. The sensor's electrical resistance was measured using a millimeter connected to a computer after placing

the sample in an enclosed chamber. The sensing measurements were taken at different temperatures. The resistance change measured the sensor's response. The following equation calculated the sensor's sensitivity upon exposure to NH3 gas:

$$S\,\% = \left|\frac{R_a - R_g}{R_g}\right| * 100\% \quad (2)$$

Where 〖R_a and R〗_g are the sensor's resistance before and after exposure to the gas, respectively.

4. Results

Structural properties of nano-composites:

X-ray diffraction (XRD) measurements confirmed the crystallization and composition of the as-prepared and annealed rGO, CuO, and rGO/CuO nanocomposites, as shown in Figure 2. From (Figure 3.a), it can be seen that the single phase of CuO (tenorite) can be observed from pure CuO with distinct diffraction peaks at 2θ equal to .508°,35.527°,38.758°,48.766°,53.563°,58.296°.61.557°,66.137°,68.076°,

72.388°,75.127° corresponding to (110), (-111), (111), (-202), (020), (202), (-113), (-311),(311),(220),(311),(-222) according to JCPDS card (00-005-0661) of CuO. The impact of GO on forming (rGO-CuO) nanocomposites can be demonstrated using XRD analysis of the samples (0.5 g, 1 g, 2 g of graphene oxide added copper nitrate). The samples are named (S1, S2 and S3) for simplicity. The XRD results of S1 show high-intensity peaks with a single copper oxide phase with lattice constant a=4.684 A° ,b=30425 A°,c=5.129 A°, which is consistent with the data from JCPDS card (00-005-0661) matches CuO. The peaks around 2θ were presented in Table (1) and well agreed with previously published studies 38. A broad and weak additional reflection peak for the hexagonal structure of graphite corresponds to 2θ of 42° (100), due to low agglomeration and disordered stacking for rGO layers in the composites 44. In the case of S2, it is clear that the pronounced sharp peak at 2θ corresponding to 36.54°(211) indicates a cubic phase of Cu2O with a d-spacing of 2.5 nm, in addition to other small peaks at 42.329° (220) and 77.417° (422) plans accordance with the JCPDS card (00-002-1067). This result was similar to that reported previously 45 when the same method was used for preparation at 100 °C. Two phases were observed for the S3 sample tenorite (CuO) and cuprite (Cu2O), and the tenorite phase was predominated. The peak corresponding to Cu2O was observed at 29° (200) according to the JCPDS card (00-002-1067) of Cu2O. Other weak and broad peaks related to GO appeared at 16° (001), 26° (002), and 42° (100). No other peaks indicated impurities in the three samples, indicating a successful preparation method. These results showed that GO and Cu (NO3)2 were partially reduced to rGO and CuO. For the GO, it can be seen that GO has a clear peak at 2θ equal to 13.7° (001), according to the previous studies [39]. In addition to another new peak at 25.65° (002), 42.76° (100) and 77.6° (110) are related to the formation of rGO. These results agreed well with the graphite JCPDS card (00-001-0646). The appearance of a peak associated with GO indicates the incomplete reduction of graphene oxide at 100 °C.

Table 1. XRD data of samples before and after annealing.

	Before annealing					After annealing				
Sample	**2θ (°)**	**d-spacing (Å)**	**(hkl)**	**FWHM (°)**	**Crystallin e size (nm)**	**2θ (°)**	**d-spacing (Å)**	**(hkl)**	**FWHM (°)**	**Crystallin e size (nm)**
S1	32.525 35.450 38.762 42.33 48.737 53.543 58.257 61.559 66.118 68.089 72.35 75.188	2.751 2.530 2.312 2.133 1.866 1.714 1.581 1.505 1.410 1.357 1.304 1.265	110 -111 111 100 -202 020 202 -113 -311 220 311 -222	0.315 0.602 0.655 0.43 0.736 0.635 0.898 0.823 0.861 0.835 0.724 0.918	25.277 13.120 11.945 17.987 10.265 11.661 8.068 8.658 8.073 8.230 9.194 7.158	32.512 35.517 38.756 48.751 53.517 58.298 61.567 66.129 68.081 72.448 75.151	2.751 2.530 2.312 1.866 1.714 1.581 1.505 1.410 1.357 1.304 1.265	110 -111 111 -202 020 202 -113 -311 220 311 -222	0.436 0.504 0.563 0.535 0.585 0.605 0.599 0.911 0.633 0.643 0.742	18.262 15.672 13.897 14.121 12.659 11.973 11.895 7.630 10.857 10.405 8.859
S2	36.541 42.409 77.524	2.463 2.133 1.231	111 200 222	0.233 0.284 0.307	33.803 27.277 21.066	432.56 535.56 538.79 748.78 953.56 558.35 761.61 866.14 968.11 5472.4 75.219	2.751 2.530 2.312 1.866 1.714 1.581 1.505 1.410 1.357 1.304 1.26	110 -111 111 202- 020 202 -113 -311 220 311 -222	0.219 0.261 0.308 0.232 0.316 0.346 0.217 0.225 0.4 0.316 0.213	36.353 30.259 25.400 32.559 23.431 20.929 32.828 30.889 17.178 21.173 30.847
S3	16.785 26.608 29.360 32.326 35.471 38.714 42.592 44.962 48.593 51.207 53.586 58.169 61.422 66.062 68.581 72.310 75.436	5.277 3.347 3.039 2.767 2.751 2.530 2.312 2.017 1.959 1.866 1.778 1.714 1.581 1.505 1.410 1.357 1.265	111 002 110 110 -111 111 100 -112 -202 112 020 202 -113 -311 220 311 -222	0.410 0.700 0.446 0.508 0.688 0.715 0.480 0.468 0.950 0.200 0.720 0.542 0.620 0.800 0.400 0.540 0.567	20.448 12.177 19.194 17.000 12.652 12.277 18.543 19.155 9.576 46.038 12.894 17.490 15.549 12.381 25.031 19.014 18.492	26.503 29.425 32.460 35.562 38.803 46.41 48.758 53.506 58.338 61.632 66.822 68.061 72.390 75.111	3.360 3.033 2.756 2.522 2.318 2.511 1.959 1.714 1.581 1.505 1.410 1.357 1.304 1.265	002 110 110 -111 111 -112 -202 020 202 -113 -311 220 311 -222	0.483 0.146 0.431 0.353 0.433 0.426 0.550 0.637 0.519 0.588 0.948 0.742 0.827 0.758	17.641 58.695 20.032 24.649 20.295 21.183 16.552 14.570 18.282 16.420 10.441 13.482 12.419 13.803
CuO	32.508 35.527 38.758 48.766 53.563 58.296 61.557 66.137 68.076 72.388 75.127	2.751 2.524 2.312 1.866 1.710 1.582 1.506 1.410 1.376 1.304 1.264	110 -111 111 -202 020 202 -113 -311 220 311 -222	0.406 0.584 0.653 0.747 0.745 0.993 0.931 1.066 0.882 1.064 1.223	21.293 14.923 13.455 12.174 12.463 9.559 10.363 9.280 11.336 9.657 8.554	32.423 35.422 38.669 48.665 53.361 58.241 61.486 66.054 67.956 72.396 75.052	110 111 111 -202 020 202 -113 -311 220 311 -222	2.758 2.531 2.362 1.869 1.751 1.583 1.507 1.414 1.378 1.304 1.265	0.400 0.576 0.649 0.644 0.690 0.688 0.793 1.022 0.858 0.985 1.038	21.582 15.114 13.543 14.127 13.452 13.788 12.161 9.672 11.646 10.428 10.068

	13.155	6.724	001	2.532	3.298	11.691	001	7.652	0.280	29.689
	25.490	3.350	002	3.686	2.307	25.504	002	3.489	0.381	22.278
rGO	42.578	2.132	100	1.546	5.759	48.775	102	1.865	0.373	24.394
	46.070	1.968	101	0.160	56.329					
	59.524	1.551	103	0.200	47.771					
	77.699	1.288	110	1.440	7.395					

To illustrate the impact of the annealing process on the nanocomposite, all samples underwent annealing in an electric furnace at a temperature of 400 °C for 2 hours. From (Figure 3. b), the XRD results for pure CuO, S1, and S3 showed increased peak intensity and sharpness, indicating increased crystallites after annealing. However, after thermal treatment, S2 showed a different cupric oxide (CuO) phase. The clear peak of rGO becomes very weak or disappears in the three samples. This can be attributed to the high intensity of CuO that suppressed rGO, which is consistent with 44,46,47. The reduction of GO was incomplete upon annealing, resulting in the weak diffraction peak. The size of the nanocomposites could be significantly altered by manipulating the quantity of GO present in the nanocomposites. These results were consistent with those in 48. Furthermore, the average crystal size increased after annealing for all samples and resulted in the growth of CuO crystals, which is consistent with previous studies 49,50. Table (1) shows the XRD data for all samples before and after annealing.

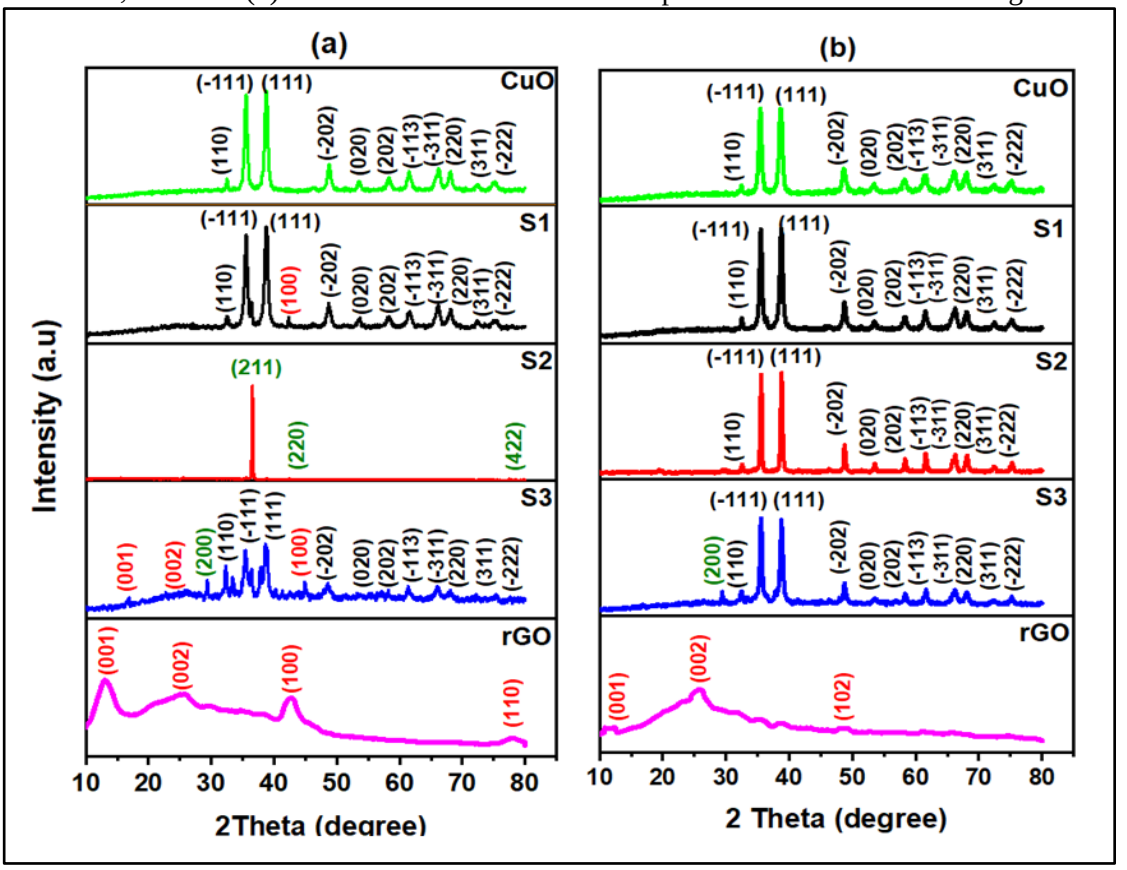

Figure 3. XRD of CuO, CuO/rGO, and rGO nanocomposites (a) as-prepared, (b) after annealing at 400 °C.

Morphological and EDX analysis of the nano-composites

The morphology of the prepared and annealed samples was analyzed in FESEM at high resolution, as shown in Figure 4. Figure (4. a,b) indicates the formation of CuO nanorods. After annealing, these structures agglomerated and condensed on the surface, appearing as larger particles. The influence of the quantity of GO on the rGO/ CuO nanocomposites was demonstrated in Figure (4c-h). S1 had a rod-shaped morphology on its surface. Upon annealing at a temperature of 400 °C, the nanorod structure undergoes aggregation, resulting in bigger particles and an unfamiliar structure.

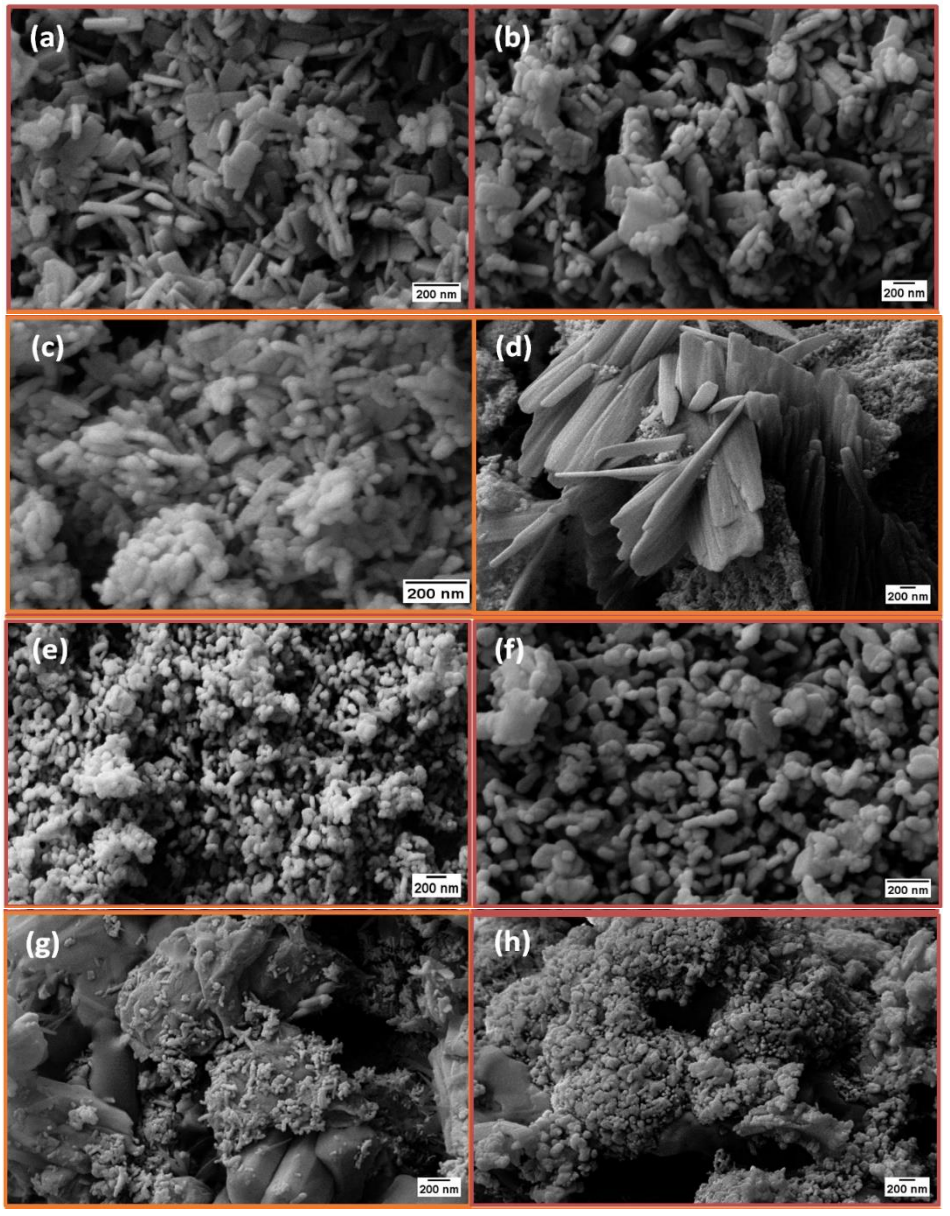

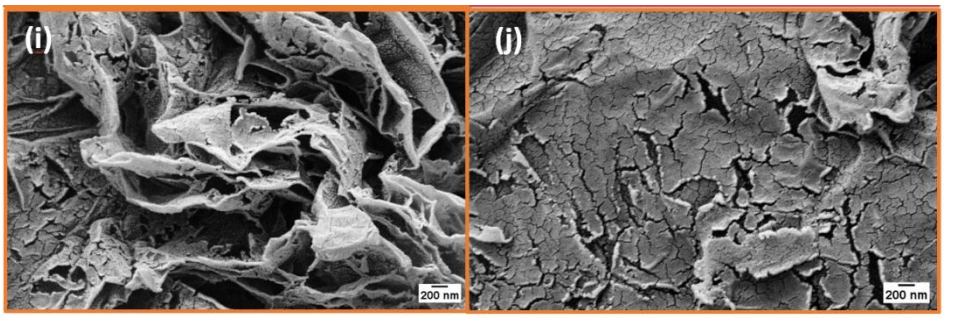

Figure 4. FESEM images of (a,b) CuO, (c,d) S1, (e,f) S2, (g,h) S3, and (i,j) rGO before and after annealing, respectively.

After increasing the amount of GO to 1 g, the nanocomposite's shape became spherical and larger after annealing. When the weight fraction of GO reaches 2 g, a semi-rod-like shape is formed, which covers the surface of the rGO sheets. After thermal treatment, this structure aggregates into large agglomerations in a spherical shape. Therefore, the number of small particles decreased and consequently increased particle size. The role of NaOH in the reaction was to establish contact between GO and CuO through hydrothermal treatment, thereby inducing electrons on the surface of GO. At this stage, the reduction of Cu+2 and GO occurs, and CuO and rGO nanocomposites are formed due to the effect of temperatures mentioned in previous works 51. All three samples were observed to have sizes in the nanoscale range. Figure (4i,j) shows the FESEM images of the as-prepared and annealed rGO. The rGO layers were agglomerated with each other in a plate-like shape, and this structure contained more defects due to the decomposition of oxygen groups after thermal annealing, indicating a reduction of GO. To prove the interstitial structure (elementary structure) of the synthetic composites previously prepared by hydrothermal method, EDX was performed and showed that Cu, O, and C are the main elements for samples Cu, S1, S2, S3, and rGO, and no other impurities are shown in Figure 5. This indicates the successful production of nanocomposites. The percentages of Cu, O, and C are shown in Table (2). The decrease in copper content in samples S1, S2, and S3 corresponds to an increase in GO concentration in the nanocomposite.

Table 2. EDX spectra of as-prepared samples.

Sample	Cu wt.%	C wt.%	O wt.%
CuO	81.6	-	18.4
S1	70.7	10.9	18.4
S2	52.5	25.7	21.8
S3	36.1	39.2	24.7
rGO	-	83.8	16.2

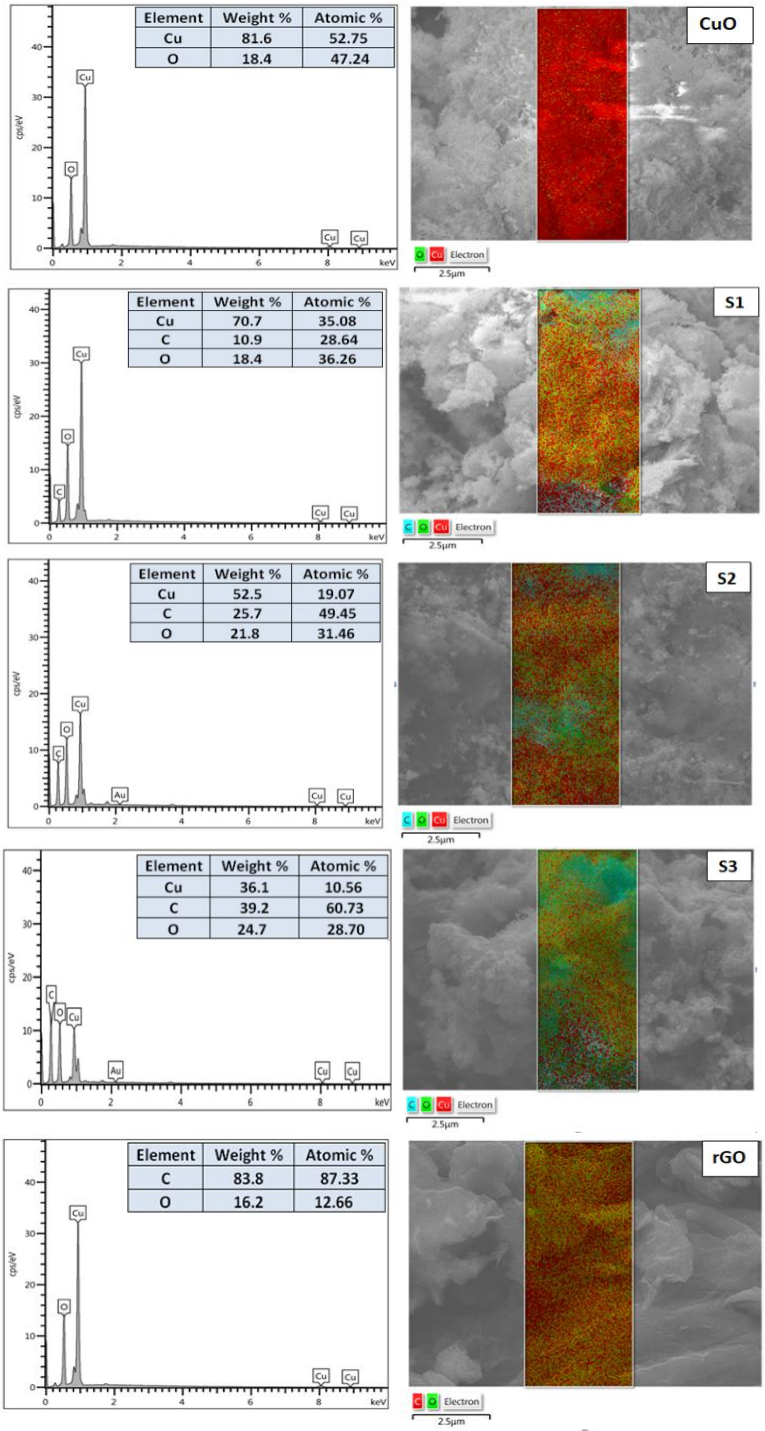

Figure 5. EDX spectrum and elemental mapping for CuO, rGO/ rGO, and rGO.

Optical properties of nanocomposites

The UV-visible absorption spectrum of all samples before and after annealing is shown in Figure 6. This spectrum was recorded for the range (190-1200 nm). From Figure 6(a), the absorption peak of samples S1, S2, and S3 is red-shifted at 293 nm, while the absorption peak of CuO appears at around 354 nm and of rGO at about 230,325 nm, indicating (π^*- π^*) and (n- π^*) transitions of the double bonds between (C = C) and (C-O) in the graphite framework 52. These two peaks appeared in reduced graphene oxide, indicating the incomplete reduction of graphene oxide. There was no significant effect of annealing on the first three samples, apart from a slight increase in absorbance. Furthermore, the absorption of CuO increased, and the peak appeared at around 324 nm. After annealing, a single peak at around 231 nm was observed for rGO, indicating a reduction of GO.

Thermogravimetric analysis (TGA):

Figure 7 shows the thermal stability of materials under a nitrogen atmosphere with a temperature rise of 50 °C 〖min〗^(-1) before and after annealing. TGA analysis of CuO showed a slight weight reduction of about 2.25% between 100 °C and 400 °C, which is due to the evaporation of volatile compounds. After reaching a temperature of 450 °C, no additional mass loss was recorded, save for a marginal decrease of 1%. This suggests that the thermal stability of CuO is approximately 450 °C. Observations of samples S1 and S2 indicate that a modest weight reduction, ranging from 5% to 7%, occurs at temperatures below 450 °C. This weight loss can be attributed to the evaporation of water in the nanocomposites. After that, the weight loss increased to about 12%, indicating the degradation of the oxygen-containing functional groups in the composite 47. No further weight loss was observed after 800 °C. However, in the case of S3, the weight loss due to absorbed moisture increased to 11% as the GO ratio in the nanocomposite increased, at around 150 °C. The gradual weight loss was 42% at 800 °C due to the combustion of carbon in the composite. The gradual weight loss was observed during the TGA of rGO between 100 °C and 200 °C. After 200 °C, there was a rapid weight loss of around 27.4% up to 250 °C in the second step. This is due to the evaporation and reduction of the carboxyl and hydroxy groups. Thermal stability was observed after 250 °C and a slight weight loss of about 4% up to 450 °C. Gradual weight loss continues until 700 °C, and the total weight loss reaches 46%.

FTIR spectroscopy

FTIR spectroscopy is utilized to identify the vibrational frequencies in the synthesized CuO, rGO/CuO, and rGO, as depicted in Figure 8. The peak detected at 3742 cm-1 was ascribed to the stretching vibrations of O–H bonds induced by water absorption in the composites. The peak observed at 2360.9 cm-1 in CuO is attributed to the stretching vibrations of CH2 47. The absorption peak seen at 659 cm-1 was likely attributed to the vibration of the Cu-O bond in the monoclinic phase of CuO 53. The rGO-CuO sample exhibits a distinct absorption band at 3447 cm−1, attributed to the stretching and bending vibrations of the hydroxyl groups and water molecules on the surface.

Furthermore, 1475 cm-1 and 520 cm-1 peaks confirmed that the cuprous ions were securely attached to the graphene oxide layers 54. The occurrence of a peak of about 1508 cm-1 in the rGO sample can be attributed to the existence of C=C in a graphene oxide sheet. Additional

peaks at 1161 cm-1, 918 cm-1, and 605 cm-1 can be attributed to rGO, indicating that the GO underwent partial reduction55.

Sensors response

The sensors' responsiveness was evaluated under different temperature conditions. The sensing performance of the rGO/ CuO nanocomposites, synthesized at 100 ℃, was evaluated. The chamber was purged with ultra-pure nitrogen gas N2 (99.9%), and measurements were taken at various temperatures (room temperature, 100 °C, 200 °C). The rGO/CuO sensors were positioned within the chamber, and Ammonia gas was introduced into the chamber at the desired concentrations. The sensing performance of the rGO/CuO sensors was evaluated by applying a voltage of 500 millivolts at ambient temperature. The sensor's sensitivity to NH3 gas was assessed using eq. (4). Figure 9 illustrated the rGO/CuO sensors response to 100 ppm NH3 gas at various temperatures. The sensor sensitivity of the three samples exhibited higher values at room temperature, with recorded values of 5.95, 9.13, and 6.42 for samples S1, S2, and S3, respectively, as evident from Figure 9 (a-c). The sensing response decreased when the temperature was subsequently raised to 100 °C. When the temperature was raised to 200 °C, there was a little increase in sensitivity for samples S1, S2, and S3. This change can be related to the release of oxygen at higher temperatures due to desorption 56. The optimal operating temperature for rGO/CuO sensors is around room temperature. Results showed that sensor response is highly influenced by the weight ratio of GO in nanocomposites. A comparison was made between hydrothermally synthesized CuO and rGO/CuO sensor gas. Figure 10 shows that the sensitivity of CuO increased with higher sensor temperatures, reaching 5.32 at 200 °C. The respond of S2 sensor was 9.13 at room temperature, significantly higher than other rGO/CuO sensors and up to threefold the CuO sensor (3.16) (see Figure 11). The rGO-incorporated CuO exhibited significantly improved sensing responsiveness compared to pure CuO. Additionally, sample S2 showed rapid response and recovery time of 21 s and 15 s, faster than previous works at room temperature 57. Table 3 displays all sensors' estimated sensitivity, response, and recovery times.

Table 3Sensitivity, response and recovery times of rGO/CuO nanocomposites and CuO.

Sample	OperationTemperature(°C)	S%	Res. time (sec)	Rec. Time (sec)
S1	RM	5.95	27	30
	100	2.46	34	31
	200	3.35	30	34
S2	RM	9.31	21	15
	100	5.66	26	29
	200	5.94	21	11
S3	RM	6.42	18	25
	100	3.55	33	19

	200	**5.83**	**25**	**15**
CuO	**RM**	**3.16**	**15**	**38**
	100	**4.49**	**28**	**18**
	200	**5.32**	**22**	**20**

Gas sensing mechanism

The adsorption of target gases on their surfaces alters the resistance of gas sensors. This phenomenon constitutes the fundamental concept of the detection process of metal-oxide gas sensors 58. Initially, we will discuss the sensing process employed in the bare CuO gas sensor. CuO is a p-type semiconductor characterized by the presence of holes as its primary charge carriers. Within the air, oxygen molecules with a significant electron affinity (0.43 eV) readily adhere to the sensor surfaces and extract electrons from the surfaces of CuO; as a result, adsorbed oxygen ions will appear on the surface in molecular (O2) and atomic (O− and O2−) forms as shown in eq.(4-7)59:

$$\boldsymbol{O_2(gas) \rightarrow O_2(ads)} \quad (4)$$

$$\boldsymbol{O_2(ads) + e^- \rightarrow O_2^-(ads)} \quad (5)$$

$$\boldsymbol{O_2^-(ads) + e^- \rightarrow 2O^-(ads)} \quad (6)$$

$$\boldsymbol{O^-(ads) + e^- \rightarrow O^{2-}(ads)} \quad (7)$$

Consequently, the rise in hole carrier concentrations leads to decreased resistance. After introducing NH3 gas, electrons will be released, interacting with CuO. Consequently, the amount of hole carriers decreases, leading to an increase in the resistance of CuO. The rGO/CuO composites exhibited remarkable reactivity to NH3. rGO/CuO has p-type semiconducting behaviors, with the conductance primarily dependent on rGO; therefore, the oxygen functional groups in rGO withdraw electrons from NH3 gas. The presence of dangling bonds and surface defects in rGO increases the number of sites available for NH3 adsorption. When rGO and CuO come into contact, electrons are transported from rGO to CuO because of the disparity in their work functions (5.3 eV for CuO and 4.7 eV for rGO) 57, causing a bending of the band at the rGO/CuO interface. Consequently, the concentration of hole carriers decreases while the resistance of rGO/CuO increases. Nevertheless, when the concentration of rGO is high enough, it creates an additional pathway for current flow, leading to a more extensive conduction path along the rGO. This, in turn, decreases the initial resistance and consequently impacts the sensor's response time compared to the optimal quantity of rGO.

5. Conclusions

A simple and cost-effective strategy for preparing CuO/rGO nanocomposites was reported. The Cu and GO were reduced using a hydrothermal method at a temperature of 100 °C. CuO and rGO were verified using XRD, EDS, and FTIR analysis and further improved using FESEM. The average particle size was calculated using Scherer's equation and was found to increase with increasing GO construction. Two structures were observed in FESEM results:

rod and spherical shapes corresponding to the GO amount in the composite. The results of TGA revealed that the as-prepared samples (S1, S2, S3) were less stable as GO weight increased compared to pure CuO and more than rGO. It was found from the results that the amount of rGO has a significant effect on the sensing performance of NH3 gas. The rGO/CuO sensors exhibited a good response of about 5.95, 9.13, and 6.42 for samples S1, S2, and S3, respectively, compared to pristine CuO, which was about 3.16 at room temperature. The S2 nanocomposite sensor demonstrated a 21 s response and 15 s recovery time to 100 ppm NH3 at 30 °C, significantly improving compared to earlier studies.

Acknowledgments

I want to thank the Department of Physics, College of Science, University of Kerbala, Kerbala, Iraq, for its assistance in accomplishing this work.

References

1. B. Paulchamy and L. Durai, J. Nanosci. Nanotechnol, 6, 1(2015).
2. H. Kazem, L. Ahmed, and M. Kareem, Egypt. J. Chem, 65, 1 (2022).
3. E. Alkhafaji, N. Oda, and L. Ahmad, Egypt. J. Chem, 65, 6 (2022).
4. A. Dey, Mater Sci Eng B Solid State Mater Adv Technol, 229, 5107 (2018).
5. P. Raju, and Q. Li, J Electrochem Soc 169, 057518 (2022).
6. T. Jawad, M. Al-Lami, A. Hassen, and L.Ahmad, Egypt J Chem, 64, 9 (2021).
7. S. Sagadevan,A. Lett, G. Kassegn, S. Gark, W. Chan, N. Hamizi, and M. Joha, Catalysts, 11, 8 (2021).
8. B. Taresh, F.Fakhri, and L. Ahmed, J Nanostru, 12, 3 (2022).
9. K. Revathi, S.Palantavida, and B. Kizhakkekilikoodayil, Mate Today, 9, (2019).
10. L. Bu, and R. Huang, Ceram. Int, 43, 1 (2017).
11. H. Abo-Dief, A. Alanazi, Z. Alothman, T. Pramanik, A. Mohamed, A. Fallata, J. Althakafy, Cryst, 12, 10 (2022).
12. S. Bhuvaneshwari, and N. Gopalakrishnan, J. Alloys Compd, 654, (2016).
13. L. Hou, C. Zhang , L. Li , C. Du, X. Li, X. Kang, and W. Chen, Talanta, 188, 9140 (2018).
14. V. Akshata Ajit,W. Gawli, A. Ethiraj, AIP Conf Proc, 1953, 030182 (2018).
15. A. Kumar, and D. Synthesis, Eur. J. Clin Med, 7, 2020 (2020).
16. K.Phiwdang, S. Suphankij, W. Mekprasart, and W. Pecharapa, Eng Procedia, 34, (2013).
17. F. Nazeer, Z. Ma, L. Gao, H.Wu, A. Malik, X.Meng C. Li, J. Long, Comp B: Eng, 163, 4 (2019).
18. A. Ballantyne, H. Alesary, H. Ismail, A.Hameid Odda, M. Watkins, A. Arkan Majhool, K. Ryder, J Electroanal Chem, 897, 115581 (2021).
19. S.Pourbeyram, J. Abdollahpour, and M. Soltanpour, Mater Sci Eng C, 94, 1 (2019).
20. G. Rena, D. Hub, E. Cheng, M. Vargas-Reus, P.Reip, R. Allaker, Int. J. Antimicrob Agents, 33, 6 (2009).
21. H. Mohammad, S.Saeed, and L. Ahmed, J Nanost, 12, 4 (2022).
22. R. Ortega-Amaya, Y. Matsumoto, A.Espinoza-Rivas, M. Pérez-Guzmán, and M. Ortega-López, Beilstein J Nanotechnol, 7, 1 (2016).
23. A. Rhazouani,H. Gamrani, M. El Achaby, K. Aziz, L. Gebrati, M. Sahab Uddin,and F. AZIZ, BioMed Res Int, 2021, 5518999 (2021).
24. G. Lu, L. Ocola, and J. Chen, Nanotechnol, 20, 445502 (2009).
25. M.Eluyemi, M. Eleruja1, A. Adedeji, B. Olofinjana, O. Fasakin, O. Akinwunmi,
26. O. Ilori, A. Famojuro, S. Ayinde, and E. Ajayi, Graphene 5, 3, (2016).

27. C. Ching Liang, and A. Zainab Ngaini, J Chem, 15, 3 (2015).
28. A. Singh, N. Sharma, M. Arif, and R. Katiyar, Electrically reduced graphene oxide for photovoltaic application. J Mat Res, 34,4 (2019).
29. S. Wu, S. Soo, and J. Hulme, Int J Nanomedicine, 10, (2015).
30. M. Hoseini-Ghahfarokhi, S. Mirkiani, N. Mozaffari, M. Amin Abdolahi Sadatlu, A.Ghasemi, S. Abbaspour, M. Akbarian, F. Farjadian, M. Karimi, Int J Nanomedicine, 2020, 15 (2020).
31. S. Saeed , B. Taresh, L. Ahmed , Z. Haboob , S. Hassan , and A. Jassim, J Chem Health Risks, 11, 4(2021).
32. L. Davoise, A. Díez-Pascual, and R.Capilla, Mat,15, 3 (2022).
33. M. Shaban, S. Ali, and M. Rabia, J Mat Res Tech, 8, 5 (2019).
34. C. Sarkar, and S. Dolui, RSC Adv, 5, 75 (2015).
35. J. Kim, A. Mirzaei, Y. Zheng, J. Lee, J. Kim, H. Kim, and S. Kim, Sens Actuators B Chem 281, 4005 (2019).
36. D., Zhang, N. Yin, C. Jiang, and B. Xi, J Mater Sci: Mater Electron, 28, 3 (2017).
37. S. Sagadevan, Z. Chowdhury, M. Johan, F. Abdul Aziz, E. Salleh, A. Hawa, and R. Rafique. J Exp Nanosci, 13, 1 (2018).
38. M.Pratheepa, and M. Lawrence,Int J Res, 5, 12 (2019).
39. H. Bai, H. Guo, J. Wang, Y. Dong, B. Liu, Z. Xie, F. Guo, D. Chen, R. Zhang, Y. Zheng. Sensors Actuators B: Chem, 337, 129783 (2021).
40. F. Alosfur, and N. Ridha, Appl Phys A, 127, 203 (2021).
41. P. Chaiyo, Sci Ess J, 39,1 (2023).
42. O. Slobodian, P. Lytvyn, A. Nikolenko , V. Naseka, O. Khyzhun , A. Vasin, S. Sevostianov and A. Nazarov, Nano Express, 13,1(2018).
43. S. Rai, R. Bhujel, J. Biswas, and B.Swain, Ceram Int, 45, 11 (2019).
44. S. Hussein, M. Mohammad, and L. Ahmed, AIP Conf Proc, 2547, 1 (2022).
45. Z. Lu, Z. Ma, P. Song, and Q. Wang, J Mater Sci: Mater Electron, 32, (2021).
46. B. Sakthivel, and G. Nammalvar, J Alloys Compd, 788, (2019).
47. S. Kumar, G. Mamatha, H. Muralidhara, M. Anantha, S. Yallappa, B.Hungund, K. Kuma J Sci: Adv Mater Devices, 2, 4 (2017).
48. S. Archana, K. Kumar , S. Olivera, B. Jayanna , H. Muralidhara, A. Ananda , and C. Vidyasagar, Energy Environ. Focus, 5, 4 (2017).
49. F. Anjum, M. Shaban, M. Ismail, S. Gul, E. Bakhsh, M. Khan, U. Sharafat, S. Khan, and M. Khan , ACS Omega, 8, 20 (2023).
50. A. Hussain, K. Hassoon, and M. Hassan, J Phys Conf Ser, 1530, (2020).
51. P. Gokuladeepan, and A. Karthigeyan, Appl Surf Sci, 449, (2018).
52. J. Sultana, S. Paul, A. Karmakar, G. Dalapati, and S. Chattopadhyay, J Mater Sci: Mater Electron, 29, 2 (2018).
53. P. Singh, P.Nath, R. Arun, S. Mandal, and N. Chanda, RSC Adv, 6, 95 (2016).
54. Y.Zhao, X. Song, Q. Song, and Z.Yin, Cryst Eng Comm, 14, 20 (2012).
55. S. Sagadevan, J. Lett , G. Weldegebrieal , S. Garg , W. Oh, N. Hamizi, and M. Johan, CATACJ, 11, 8 (2021).
56. R.Chuah, S.Gopinath, P. Salimi, A. Radi, W. Yaakub, and T.Lakshmipriya, 3 Biotech, 10, 8 (2020).
57. C.Wang, L. Yin, L. Zhang, D. Xiang, and R. Gao, Sens, 10, 3 (2010).
58. B. Sakthivel, and G. Nammalvar, J Alloys Compd, 788, 422–428 (2019).
59. J. Kim, Ali Mirzaei, Y. Zheng, J. Lee, J. Kim, H. Kim, and S. Kim, Sensors Actuators B: Chem, 281, (2019).
60. S. Davarpanah, R. Karimian, V. Goodarzi, and F. Piri, J Appl Biotechnol Rep, 2, 4 (2015).